PCCP

Lithium Transference in Electrolytes with Star-Shaped Multivalent Anions Measured by Electrophoretic NMR

Journal:	*Physical Chemistry Chemical Physics*
Manuscript ID	CP-ART-02-2023-000923.R2
Article Type:	Paper
Date Submitted by the Author:	08-Jun-2023
Complete List of Authors:	Chakraborty, Saheli; Lawrence Berkeley National Laboratory, Material Sciences Division; University of California Berkeley, Department of Chemical and Biomolecular Engineering; Lawrence Berkeley National Laboratory, Joint Center for Energy Storage Research (JCESR) Halat, David; Lawrence Berkeley National Laboratory, Materials Sciences Division; University of California Berkeley, Department of Chemical and Biomolecular Engineering; Lawrence Berkeley National Laboratory, Joint Center for Energy Storage Research (JCESR) Im, Julia; University of California Berkeley, Department of Chemical and Biomolecular Engineering Hickson, Darby; University of California Berkeley College of Chemistry Reimer, Jeffrey; UC Berkeley, Chem and Biomolecular Engineering Balsara, Nitash; University of California, Chemical and Biomolecular Engineering

Lithium Transference in Electrolytes with Star-Shaped Multivalent Anions Measured by Electrophoretic NMR

Saheli Chakraborty*,[1,2,3] David M. Halat*, [1,2,3] Julia Im,[2] Darby T. Hickson,[1,2,] Jeffrey A. Reimer,[1,2,3] Nitash P. Balsara[1,2,3]

1. Materials Sciences Division, Lawrence Berkeley National Laboratory, Berkeley, California 94720, United States
2. Department of Chemical and Biomolecular Engineering, University of California, Berkeley, Berkeley, California 94720, United States
3. Joint Center for Energy Storage Research (JCESR), Lawrence Berkeley National Laboratory, Berkeley, California 94720, United States

* Both the authors contributed equally

Abstract

One approach for improving lithium transference in electrolytes is through the use of bulky multivalent anions. We have studied a multivalent salt containing a bulky star-shaped anion with a polyhedral oligomeric silsesquioxane (POSS) center and lithium counterions dissolved in a solvent. The charge on each anion, z_- is equal to -20. The self-diffusion coefficients of all species were measured by pulsed field gradient NMR (PFG-NMR). As expected, the anion diffusion was significantly slower than the cation diffusion. An approximate transference number, also referred to as the current fraction (measured by Bruce, Vincent and Watanabe method), was higher than those expected from the PFG-NMR. However, the rigorously defined cation transference number with respect to the solvent velocity measured by electrophoretic NMR was negative at all salt concentrations. In contrast, the approximate transference numbers based on PFG-NMR and current fractions are always positive, as expected. The discrepancy between these three independent approaches for characterizing lithium transference suggests the presence of complex cation–anion interactions in solution. It is evident that the slow self-diffusion of bulky multivalent anions does not necessarily lead to an improvement of lithium transference.

Introduction

There is significant interest in multivalent electrolytes due to their relevance in rechargeable batteries.[1–6] Electrolytes used in lithium-ion batteries comprise univalent ions dissolved in a mixture of organic solvents. Lithium transference in these electrolytes is low, implying that a large fraction of the current is carried by the anions.[7,8] It has been postulated that bulky multivalent anions may lead to improvement of lithium transference.[9–11] In a recent study, Nguyen et al. studied ion transport in solutions containing bulky multivalent star-shaped anions where one also expects ion transport to be dominated by that of the cation.[1]

Irrespective of the valency of the ions, the performance of binary electrolytes, comprising two ions and a solvent, in batteries depends on three transport parameters: ionic conductivity, κ, salt diffusion coefficient, D, and cation transference number, t_+^0. The purpose of this paper is to study lithium transference in a solution comprising star-shaped multivalent anions presenting a valency of -20, univalent Li^+ counterions, and a low molar mass solvent – a mixture of ethylene carbonate (EC) and dimethyl carbonate (DMC). The transference number, t_+^0, is defined as the fraction of current carried by the cation relative to the solvent velocity.[12–14] The most popular approach to study lithium transference is one wherein the electrolyte is sandwiched between two lithium metal electrodes and the current i under a steady applied potential $\Delta\phi$ is monitored as a function of time. Following the work of Bruce, Vincent, and Watanabe et al.,[15–17] we define the current ratio ρ_+ as the ratio of steady state current (i_{SS}) to that of the initial current (i_0)

$$\rho_+ = \frac{i_{SS}}{i_0}. \quad (1)$$

Equation 1 is valid when the current through the cell is dominated by bulk impedance (not interfacial impedance). While the currents depend on the magnitude of $\Delta\phi$, ρ_+ is a material property that is independent of $\Delta\phi$ when the applied potentials are sufficiently small. Another approach for determining transference number employs pulsed field gradient NMR (PFG-NMR) which can be used to measure the self-diffusion coefficients of the cations and anions, D_+ and D_-.[18] The PFG-NMR-based cation transference number can be defined as

$$t_{+,PFG} = \frac{z_+ D_+}{z_+ D_+ - z_- D_-}. \quad (2)$$

Here, z_j represents the charge on species j (valency).[19]

In the limit of infinite dilution, t_+^0, ρ_+, and $t_{+,PFG}$ must be equal to each other.[20,21] At finite concentrations, however, the relationships between these parameters is nontrivial; they depend on other transport and thermodynamic parameters that reflect correlations between different species.[12,22]

An alternative approach for measuring t_+^0 is electrophoretic NMR (eNMR).[23–32] In this approach, pioneered by Zawodinski and coworkers,[27,28] a steady electric potential $\Delta\phi$ is applied across the electrolyte and the displacement of the NMR-active species in a fixed time window is measured by quantifying spectral phase shifts. This enables determining species velocities that are directly related to t_+^0. For the case of univalent ions,[24,25] it was shown that

$$t_+^0 = \frac{v_+ - v_0}{v_+ - v_-}. \quad (3)$$

Here, v_+, v_- and v_0 are the average velocities of cation, anion and solvent, respectively. While the species velocities are proportional to $\Delta\phi$, t_+^0 is a dimensionless material property that is independent of $\Delta\phi$ when the applied potentials are sufficiently small.

The salt we have chosen for our study is lithiated polyhedral oligomeric silsesquioxane (POSS) nanoparticles (Figure 1). These nanoparticles can be thought of as eight-armed stars with two or three anions in each arm, yielding $z_- = -20$. A similar salt with z_- ranging from 6.6 to 10 was studied by Bouchet and coworkers where they report high PFG-NMR-based cation transference numbers.[1] While the star-shaped anions are similar to charged dendrimers that have been studied in prior literature,[33–38] we are not aware of any measurements of transference in solutions of such systems. In the present work our main objective is to study the relationship between t_+^0, ρ_+, and $t_{+,PFG}$ in our multivalent POSS system.

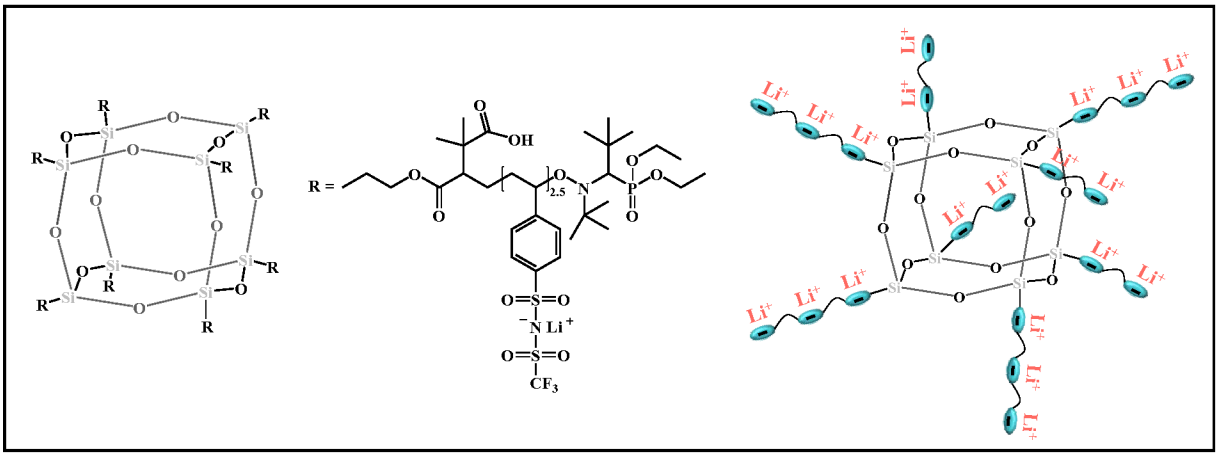

Figure 1. Chemical formula of the polyanionic electrolyte based on POSS. The average number of negative charges on the POSS nanoparticle is 20.

Experimental Section

Preparation of electrolyte

The POSS nanoparticles containing lithium salt of polystyrene-4-sulfonyl(trifluoromethane sulfonyl) imide (POSS-PSLiTFSI) were synthesized following the previous literature report.[39] The salty nanoparticles were dried at 100 °C under active vacuum for 72 hours. The salt was stored under argon in a glovebox where water and oxygen levels were kept below 0.5 ppm before further use.

The electrolytes were prepared inside the glovebox by adding the required amount of POSS-PSLiTFSI to the dry ethylene carbonate (EC) and dimethyl carbonate (DMC) mixture (1:1 by weight) and stirring the solution at 60 °C overnight in an airtight container.

The concentrations of the electrolytes were determined by NMR. ^{7}Li NMR spectra of solutions of LiTFSI salt in N-methylpyrrolidone with concentrations ranging from 0.05 to 1 mol/L were measured and the peak intensities were used to generate a calibration curve. A recycle delay period of 5 sec was applied between each NMR scan to ensure complete relaxation of the species. A total of 8 scans were performed in each NMR experiment. The calibration curve is shown in Figure 2. Mixtures of POSS-PSLiTFSI/EC/DMC with known mass fractions of POSS-PSLiTFSI were prepared and the ^{7}Li peak intensities from these solutions were measured. The measured

intensities were compared with the calibration curve as shown in Figure 2 and this enables determining the molar concentrations of lithium ions, c_+. The c_+ values thus obtained are 0.071, 0.21, 0.40, 0.53 and 0.73 mol/L. These NMR experiments also enable calculation of the average number of lithium ions per POSS particle in each electrolyte. Data obtained from all five solutions were used to determine the average valency of the anions. This analysis gave $z_- = -20 \pm 2$. This implies that the average number of monomers per chain is 2.5 assuming that the chains emanate from all eight corners of the POSS particles.

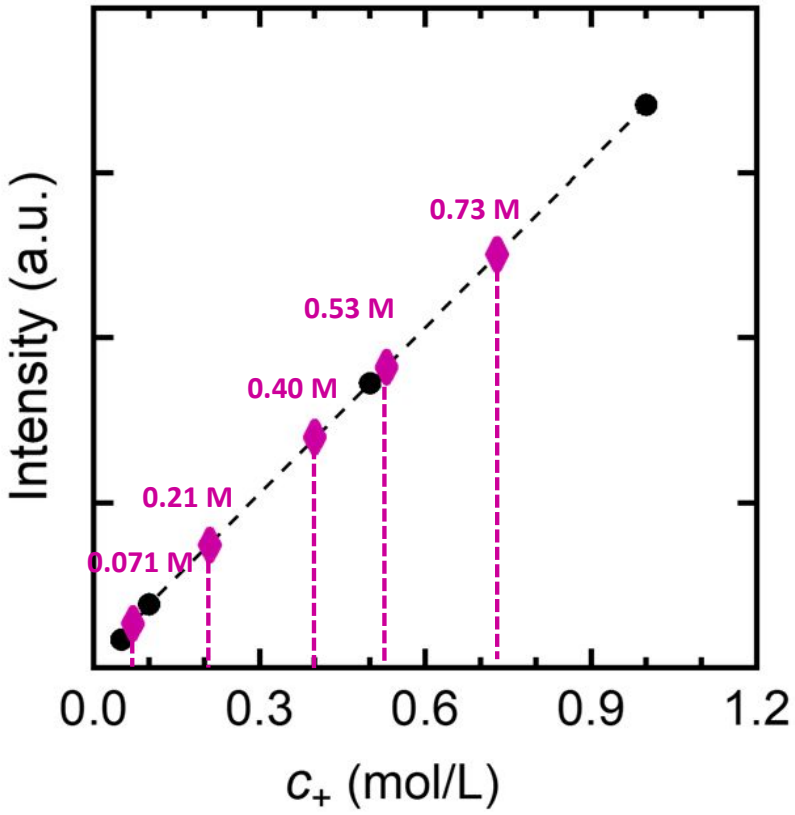

Figure 2. Determination of salt concentration by ^{7}Li NMR spectroscopy. The y-axis represents the intensity of the NMR spectra and the x-axis represents the concentration of lithium salt. The data points in black circles and the connected black dotted lines represent the calibration curve with different LiTFSI salt concentrations. Magenta diamonds represent the POSS-PSLiTFSI data and the vertical line to the x-axis represents the determined concentration. The numbers in the figure represent c_+ of the electrolytes used in this study.

Electrochemical characterization

Conductivity measurements

Conductivity of the electrolytes were measured with a Mettler Toledo InLab-751 conductivity probe with platinum blocking electrodes. The temperature of the electrolytes was measured using the probe and was maintained at 30 ± 1 °C during the measurements. Each measurement was carried out three times to ensure reproducibility. The conductivity probe was calibrated prior to the experiment using a potassium chloride standard with conductivity 1413 μS/cm to determine the cell constant.

Current fraction measurement

The current fraction was determined using Li/POSS-PSLiTFSI(EC/DMC)/Li symmetric cells assembled in coin cell conformation. Five layers of Celgard 2500 separators were soaked in the electrolyte and stacked between lithium chips of 14 mm diameter and 600 μm thickness (MTI Corp.). The cell stack was backed with a stainless-steel shim of diameter 15.5 mm and a wave spring before crimping. At least three to four cells were made at each salt concentration to check reproducibility. The cells were cycled at 30 °C inside an environmental chamber connected to a thermocouple.

The cells were preconditioned by polarizing at 0.02 mA/cm^2 for four hours in both positive and negative directions followed by one hour of open circuit potential relaxation steps between each of the polarization steps. Five preconditioning cycles were carried out to ensure the formation of stable solid electrolyte interphase (SEI) between the lithium metal and the electrolyte. After that the cells were polarized at $\Delta\phi$ = 10 mV, -10 mV, 20 mV and -20 mV to ensure that the measurements were independent of applied potential. The steady state current, i_{SS}, was measured for 1 hour and the impedance was monitored before ($R_{b,0}$, $R_{i,0}$) and after the polarization ($R_{b,SS}$, $R_{i,SS}$,). R_b and R_i represent the bulk and interfacial resistances, respectively. The initial current density is determined based on Ohm's law assuming the absence of any concentration gradient at the initial instant of polarization as

$$i_{\Omega} = \frac{\Delta\phi}{R_{i,0} + R_{b,0}} \ . \quad (4)$$

The current fraction was determined using the following equation[15–17]

$$\rho_{+} = \frac{i_{SS}}{i_{\Omega}} \left(\frac{\Delta\phi - i_{\Omega} R_{i,\,0}}{\Delta\phi - i_{SS} R_{i,SS}} \right). \quad (5)$$

Equation 5 is an extension of equation 1 for the case when interfacial impedance cannot be neglected.

Pulsed-field-gradient NMR

All ^{7}Li, ^{19}F, and ^{1}H NMR experiments were performed at a field strength of 9.4 T using a 400 MHz Bruker NEO spectrometer and a Bruker 5 mm water-cooled double resonance broadband diffusion (diffBB) probe, which was equipped with z-axis gradient capabilities permitting a maximum gradient strength of 17 T/m and variable-temperature control. The observed ^{7}Li and ^{19}F resonances unambiguously corresponded to Li^{+} cations, and to the polyanions, respectively; the ^{1}H resonances corresponding to the carbonate solvents were chosen for analysis. For PFG experiments, a standard stimulated-echo sequence (diffSte) using sine-bell magnetic field gradient pulses was employed, wherein only the gradient strength was varied for each measurement; spoiler gradient pulses of 2 ms and a longitudinal eddy current delay (LED) period of 20 ms were used for all experiments. Additionally, dummy gradient pulses were performed prior to the first spectral acquisition. Typical ^{19}F, ^{7}Li and ^{1}H PFG parameters, i.e., gradient pulse length (δ), diffusion time (Δ), and maximum gradient strength (g) were equal to or ranged as follows: δ = 1 ms, Δ = 20 ms, g = 1.4–5.3 T/m (^{1}H); δ = 1.5 ms, Δ = 50 ms, g = 2.0–12.8 T/m (^{19}F); δ = 1 ms, Δ = 50 ms, g = 4.1–9.8 T/m (^{7}Li). All measurements were performed at a calibrated sample temperature of 30 °C. Temperature and pulsed field gradient strength calibrations were performed with a standard consisting of 80% ethylene glycol in DMSO-d6 (Cambridge Isotope Labs), using the known ^{1}H self-diffusion coefficient of ethylene glycol at the calibrated temperature.[40] Data were processed and analyzed in Bruker TopSpin 3.6 and/or 4.1, and Bruker Dynamics Center.

Electrophoretic NMR

The electrophoretic NMR (eNMR) instrumentation employed in this work is based upon the setup described by Fang et al.,[41] and was supplied by P&L Scientific Instrument Service (www.plscientific.se; Lidingö, Sweden); details of our eNMR measurements have been previously reported in detail.[25] All electrolyte samples were loaded into the eNMR cell within the argon-filled glovebox used for electrolyte preparation; the cells were previously dried at 60°C overnight. We used a convection-compensated double stimulated echo (DSTE) PFG-NMR sequence,[42] with electric field pulses of opposite polarity applied during the two halves of the sequence.[43–45] Typical applied voltages ranged from 10–160 V. Although a range of electric fields were applied, in this work all eNMR species velocities are reported relative to an applied electric field of -1 V/mm. For all experiments, the drift time Δ during which the electric field was applied was fixed at 100 ms. Typical recycle delays were 60–120 s, to allow for equilibration following the electric field pulses. The calibrated sample temperature was 30°C for all measurements. Calibration of the electric field was previously performed with a 10 mM solution of tetramethylammonium bromide (TMABr) in D_2O (supplied by P&L Scientific) at 25°C. Analysis of eNMR phase shifts was performed as previously described[25] using an automated procedure comparing the "phase spectra" of the eNMR data**.**

Theory

In this section, we derive expressions that are necessary to interpret experimental data from multivalent systems. Our derivations are built on the approach described in ref. 24. We assume that we have a one-dimensional system with a potential $\Delta\phi$ applied across an electrolyte of length L (Figure 3). We are interested in predicting the initial species velocities before the onset of concentration polarization. Under these conditions, the gradient of the electric field inside the electrolyte, $\nabla\phi$, is given by $-\Delta\phi/L$.

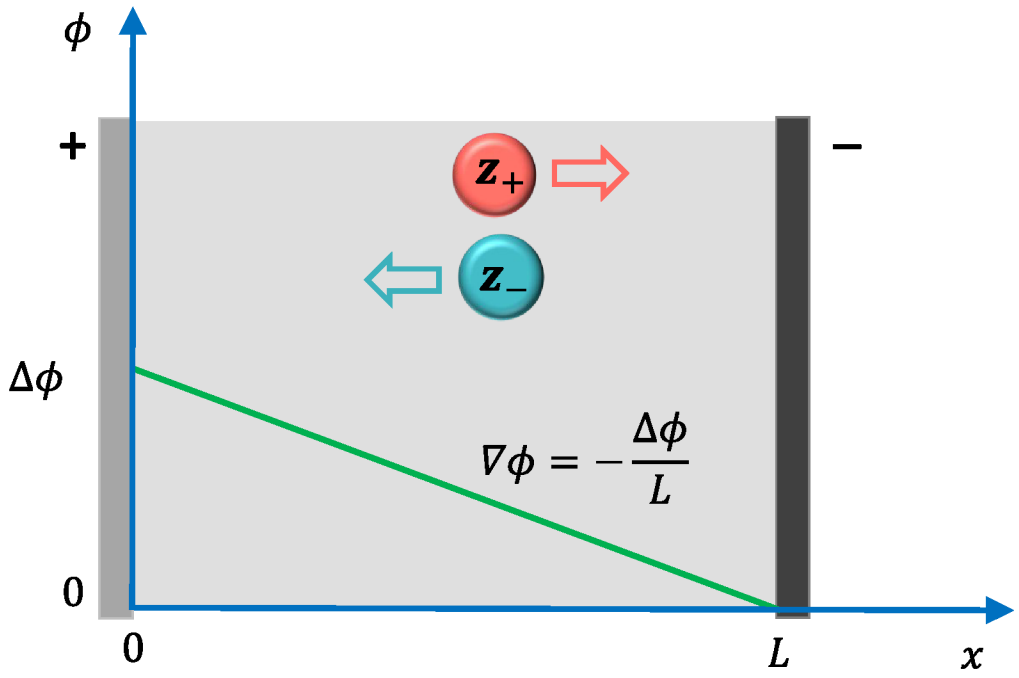

Figure 3. Schematic of the eNMR cell where a positive potential $\Delta\phi$ is applied at $x = 0$. The potential of the negative electrode is set to zero. The direction of migration of the dissociated ions is shown by the arrows (red and teal). The potential gradient driving the ion motion is given. The solution concentration is uniform, independent of x.

We use concentrated solution theory to derive the necessary equations.[12] In this theory, the Stefan-Maxwell approach is used to describe transport which is driven by the gradients of the electrochemical potentials, μ_j. Equations 10, 11 and 12 from ref. 24 are:

$$c_+\nabla\mu_+ = \frac{RTc_+c_0}{c_T\mathcal{D}_{0+}}(v_0 - v_+) + \frac{RTc_+c_-}{c_T\mathcal{D}_{+-}}(v_- - v_+) \quad (6)$$

$$c_-\nabla\mu_- = \frac{RTc_-c_0}{c_T\mathcal{D}_{0-}}(v_0 - v_-) + \frac{RTc_+c_-}{c_T\mathcal{D}_{+-}}(v_+ - v_-) \quad (7)$$

$$c_0\nabla\mu_0 = \frac{RTc_-c_0}{c_T\mathcal{D}_{0-}}(v_- - v_0) + \frac{RTc_+c_0}{c_T\mathcal{D}_{0+}}(v_+ - v_0) \quad (8)$$

where $\mathcal{D}_{jk}$ are Stefan-Maxwell diffusion coefficients, c_j are the species concentrations, and c_T is the total solution concentration. The velocities given in equations 6 – 8 reflect averages over all

of the different environments (dissociated ions, ion pairs, solvent separated ion pairs, charged triplets, etc.). Molecular-scale simulations are usually used to identify these environments, and the correspondence between the continuum and molecular approaches has been established in several previous publications.[25,46–49]

Using quasi-electrostatic potentials in an electrolyte of uniform composition,[12] we have

$$\nabla\mu_+ = z_+ F\nabla\phi \quad (9)$$

$$\nabla\mu_- = z_- F\nabla\phi \quad (10)$$

$$\nabla\mu_0 = 0 \quad (11)$$

Combining equations 8 and 11, and noting that $c_+ = c\nu_+$ and $c_- = c\nu_-$, where ν_j are the moles of ions produced by dissociation of one mole of electrolyte, we get

$$\frac{\mathcal{D}_{0+}}{\mathcal{D}_{0-}} = -\frac{\nu_+(v_+ - v_0)}{\nu_-(v_- - v_0)} \quad (12)$$

The transference number is defined in terms of the Stefan-Maxwell diffusion coefficients as

$$t_+^0 = \frac{z_+\mathcal{D}_{0+}}{z_+\mathcal{D}_{0+} - z_-\mathcal{D}_{0-}} \quad (13)$$

where z_j is the charge of species j. Substituting equation 12 into equation 13, and noting that $z_+\nu_+ = -z_-\nu_-$, we get

$$t_+^0 = \frac{v_+ - v_0}{v_+ - v_-}. \quad (14)$$

The absence of z_j in equation 14, in spite of their presence in the definition of t_+^0 in equation 13, is noteworthy. In other words, the expression for t_+^0 for multivalent ions is identical to that for univalent ions (equation 3).

The fact that ρ_+ reduces to t_+^0 in the limit of infinite dilution for both univalent and multivalent ions was proved in ref. 22. This is the justification for equation 1. Equation 2 is

obtained by replacing the Stefan-Maxwell diffusion coefficients in equation 13 by self-diffusion coefficients. Thus, we have justified all of the equations presented in the introduction.

In concentrated solution theory, conductivity is given by (equation 12.23 in ref. 12):

$$\frac{1}{\kappa} = -\frac{RT}{c_T z_+ z_- F^2}\left(\frac{1}{\mathcal{D}_{+-}} + \frac{c_0 t_-^0}{c_+ \mathcal{D}_{0-}}\right) \quad (15)$$

Substituting equations 6 and 9 into equation 15 gives (after some algebra)

$$\kappa = \frac{c_T z_+ \nu_+ (v_- - v_+)}{\nabla\phi} = \frac{c_+ z_+ (v_- - v_+)}{\nabla\phi}. \quad (16)$$

Note that in Figure 3, we assume that $\nabla\phi$ is negative. While we conduct eNMR experiments at different values of $\nabla\phi$, all of the reported species velocities are scaled to $\nabla\phi$ = -1 V/mm. In this case we expect v_+ to be positive and v_- to be negative if the salt dissociates into free anions and cations. The two velocities thus make additive contributions to κ which is always positive.

Equations 14 and 16 are the main results of our analysis. We will use these equations along with equations 1 and 2 to analyze data from our POSS-PSLiTFSI/EC/DMC electrolyte. While velocities depend on the reference frame used to measure them, they appear in equations 14 and 16 in combinations that are independent of the reference frames. Our treatment assumes the solutions contain 3 species: cations, anions and solvent. We ignore the polydispersity of the anion. We also ignore the complications arising from the presence of a mixture of solvents.

Results and Discussion

Figure 4 shows the concentration dependence of the PFG-NMR-based self-diffusion coefficients of the four species of interest, the Li^+ cation, the POSS-PSTFSI^{20-}, EC, and DMC (D_+, D_-, $D_{0,EC}$ and $D_{0,DMC}$). We have chosen c_+, the molar concentration of Li^+ ions per unit volume of solution, as a measure of salt concentration. Note that c_+ appears naturally in the

expression for conductivity (see equation 16). The overall trends seen in Figure 4 are not surprising. The solvent diffusion coefficients are largest, followed by D_+ which is significantly higher than D_- at all salt concentrations. Some of the differences in ion self-diffusion coefficients can be explained by the difference in molar masses of Li^+ (7 g/mol) and POSS-PSTFSI^{20-} (10,648 g/mol). Note however that in the dilute limit, D_+ is only a factor of 2 larger than D_-. One might expect a larger factor based on the ratio of molar masses (1500). The PFG-NMR data suggest the presence of complex interactions between ions. The diffusion of Li^+ is slower than that of the solvents in spite of the fact that the solvent molecules have larger molar masses. This effect, which arises due to coordination between Li^+ and solvent molecules, is consistent with all previous PFG-NMR studies of electrolytes.[18,20] The diffusion coefficients of all the species decrease with increasing salt concentration due to an increase in frictional interactions.[20,50] While D_+ decreases more-or-less linearly by a factor of 5, D_- decreases more sharply when c_+ exceeds 0.40 mol/L. The overall decrease in D_- over our concentration window is a factor of 20. One might expect the dependence of D_- on concentration in the dilute limit, wherein the anions are widely spaced, to be different from that in the semi-dilute regime, wherein the anions overlap with each other. If we assume that the crossover from dilute to semi-dilute occurs at $c_+^* = 0.40$ mol/L (i.e., $c_-^* =$ 0.40/20 = 0.02 mol/L), the size (length R) of the anion is estimated at 4.4 nm, $R = (N_{AV} c_-^*)^{-1/3}$, where N_{AV} is Avogadro's number. This is commensurate with the chemical structure shown in Figure 1 suggesting that the star-shaped anions are "entangled" with each other in the $c_+ > 0.40$ mol/L concentration range. We will use the data in Figure 4 in conjunction with equation 2 to obtain the concentration dependence of $t_{+,PFG}$.

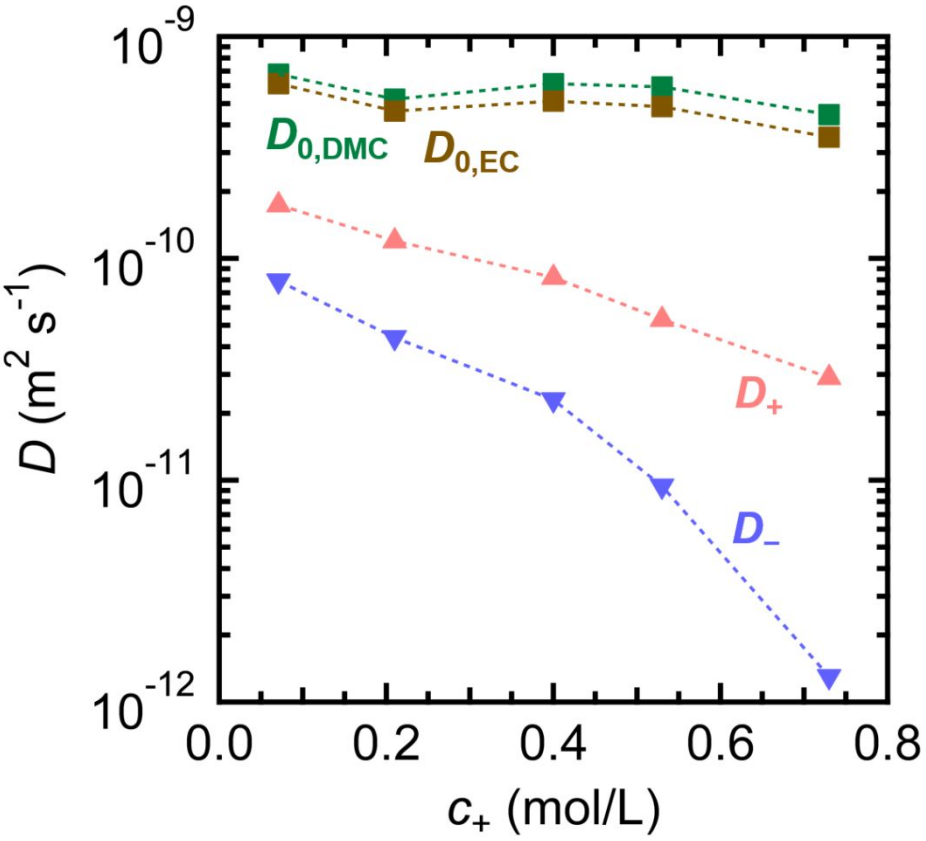

Figure 4. Self-diffusion coefficients of cation (up triangle, pink), polyanion (down triangle, blue) and solvents (square, green for DMC; square, brown for EC) measured by PFG-NMR as a function of salt concentration at 30 °C.

Figure 5 shows the concentration dependence of the eNMR-based electric-field induced species velocities at -1 V/mm of the four species of interest: the Li^+ cation, the POSS-PSTFSI^{20-}, EC, and DMC (v_+, v_-, $v_{0,EC}$ and $v_{0,DMC}$). Both the cation (v_+) and polyanion (v_-) velocities are negative at all electrolyte concentrations: the cations migrate towards the positive electrode under the applied electric field. The magnitudes of these velocities decrease with increasing concentration, consistent with the increase in frictional interactions. While the solvent velocities ($v_{0,EC}$ and $v_{0,DMC}$) are close to zero at all concentrations, the magnitudes of v_+ and v_- decrease with salt concentration up to $c_+ = 0.40$ mol/L. At $c_+ = 0.40$ mol/L, v_+ approaches zero and is comparable to the solvent velocity. Increasing c_+ further to 0.53 mol/L results in a slight increase in the magnitude of v_+. In contrast, the magnitude of v_- decreases monotonically throughout our

concentration window. At the highest salt concentration, $c_+ = 0.73$ mol/L, we arrive at the interesting situation where $v_+ \approx v_-$; both the magnitudes and the signs of the ion velocities are identical (or nearly so).

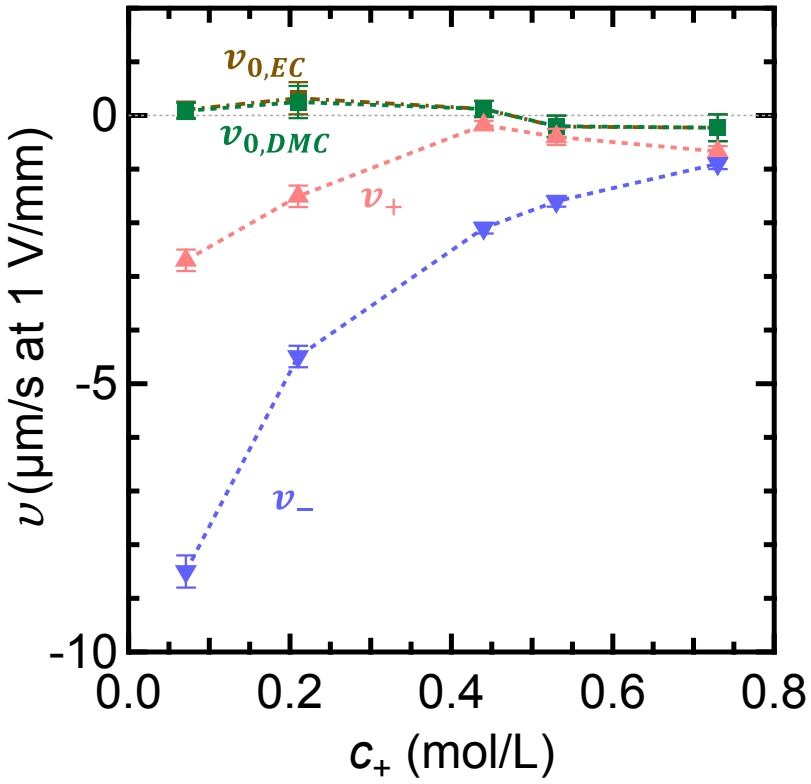

Figure 5. Average species velocities measured by ^{7}Li, ^{1}H, and ^{19}F electrophoretic NMR (eNMR) at 30 °C as a function of salt concentration, cation velocity (up triangle, red), polyanion velocity (down triangle, blue) and solvent velocities (square, green for DMC; square, brown for EC) at an applied field $\nabla\phi$ = -1 V/mm.

In Figure 6, we plot the ac-impedance-based conductivity, κ, as a function of salt concentration. The increase in κ with increasing c_+ at low concentrations ($c_+ < 0.40$ mol/L) is due to an increase in charge carrier concentration. However, frictional interactions also increase with increasing c_+. Above $c_+ = 0.40$ mol/L, the increase in frictional interactions dominate and κ decreases with increasing concentration. These data are consistent with the extensive literature

of monovalent salts dissolved in solvents.[20,51,52] We can also calculate κ using the eNMR data in Figure 5 and equation 16. These values are also shown in Figure 6. The agreement is reasonable at all concentrations. Our theoretical framework, which is based on concentrated solution theory of binary electrolytes, does not account for the polydispersity of the salt. For example, equation 16, used to calculate κ from the eNMR data, is an approximation for a polydisperse system. Equation 16 is derived from equation 15 assuming a fixed value of z_- whereas polydispersity will lead to a range of values. We posit that the deviations between the two sets of data in Figure 6 is due to this.

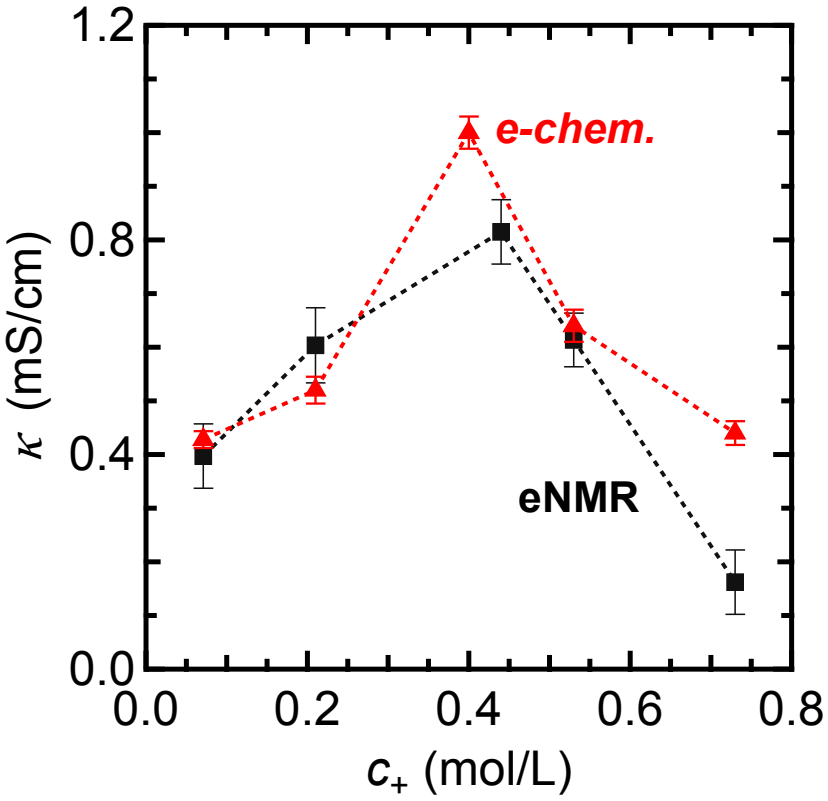

Figure 6. Ionic conductivity at 30 °C measured as a function of salt concentration using two independent methods: electrochemical method (up triangle, red) and eNMR method (square, black)

Figure 7 compares cation transference numbers using the three independent methods. The current fraction value (ρ_+), measured electrochemically, is found to be constant around 0.55 for

all salt concentrations except at the highest salt concentration, where the value decreases slightly to 0.51. This suggests that lithium transference decreases only slightly as c_+ increases from 0.53 to 0.73 mol/L. The fact that this value is significantly higher than values obtained with univalent lithium salts, which range between 0.3 and 0.4,[8,29,51,53,54] suggests that lithium transference has generally improved due to the presence of the bulky POSS-PSTFSI^{20-}. The transference number measured by the PFG-NMR ($t_{+,PFG}$) method is 0.15 in the $c_+ \leq$ 0.40 mol/L regime and increases sharply to overlap with ρ_+ at $c_+ =$ 0.73 mol/L. This observation by itself suggests that lithium transference increases sharply when c_+ increases from 0.53 to 0.73 mol/L, a conclusion which is at odds with that based on ρ_+. At most concentrations, the current supported by our electrolyte is significantly higher than that expected from $t_{+,PFG}$. It is obvious that the motion of ions under an applied potential is very different from the self-diffusion of ions in the absence of an applied potential.

The last measure of cation transference that we wish to discuss is t_+^0. We calculate this quantity using equation 14, assuming that v_0 is the average velocity of the two solvents. The surprising result is that t_+^0 is negative at all salt concentrations, a result that cannot be anticipated from either steady-state current measurements nor PFG-NMR. This finding is consistent with negative transference numbers observed by eNMR in analogous liquid electrolytes.[23] A quantitative molecular level understanding of the differences between t_+^0, ρ_+ and $t_{+,PFG}$ is outside the scope of this paper. The fact that they differ substantially from each other across the concentration range studied indicates that our data are well-removed from the infinite dilution limit where agreement between the 3 parameters is expected.[21] In an attempt to provide a qualitative explanation for negative t_+^0 values, we posit that the Li^+ counterions are in two states: a fraction of the ions f are fully dissociated and migrate freely under the electric field in the $+x$ direction, while the remainder are tightly coordinated with the anions in accordance with the principle of Manning condensation,[55–59] and migrate with anions in the $-x$ direction (Figure 3). Let us call the migration velocity of the free cations v_{f+}. The measured value of v_+ reflects a weighted average of these two populations.

$$v_+ = f v_{f+} + (1-f) v_- \quad (17)$$

The negative value of t_+^0 indicates that the overall mobility of the cations is dominated by the condensed counterions implying that the second term on the right side of equation 17 is larger than the first term. Assuming $v_0 \approx 0$ (Figure 5) for simplicity, t_+^0 is given by

$$t_+^0 = \frac{f v_{f+} + (1-f)v_-}{f v_{f+} + (1-f)v_- - v_-} \quad (18)$$

Equation 18 contains two unknown parameters, f and v_{f+}, and we expect both parameters to be functions of c_+. Measurement of cation transference alone does not permit determining both these parameters. Detailed computer simulations and additional experiments are necessary to test the validity of our hypothesis and provide a consistent explanation for the observed relationships between ρ_+, $t_{+,PFG}$ and t_+^0. In this preliminary analysis we mainly want to show that this framework provides a reasonable explanation for our observations of negative t_+^0. For example, at $c_+ = 0.071$ mol/L, if we assume $f = 0.5$ then the measured values of t_+^0 and v_- give $v_{f+} = 3$ μm/s based on equation 18. This possible value of v_{f+} is positive, and several times smaller in magnitude than the anion velocity, which is consistent with eNMR measurements of fully dissociated electrolytes.[25] In Figure S1 in the SI, we provide values for v_{f+} for other possible values of f.

Conductivity is proportional to the difference between the cation and anion velocities (equation 16). In most electrolytes, these velocities are in the opposite directions, resulting in additive contributions to the conductivity. We have shown that this is not the case for POSS-PSTFSI[20]-based electrolytes. Here v_+ and v_- are both negative at all values of c_+ and thus the ion velocities do not contribute additively to conductivity. At $c_+ = 0.73$ mol/L, we find that $v_+ \approx v_-$, and our analysis gives a value of -2 for t_+^0. There is, however, significant uncertainty due to the fact that the denominator of equation 14 approaches zero. Using standard error propagation, we obtain $t_+^0 = -2 \pm 2$ at $c_+ = 0.73$ mol/L. Molecular dynamics simulations may provide some insight into this unusual case.

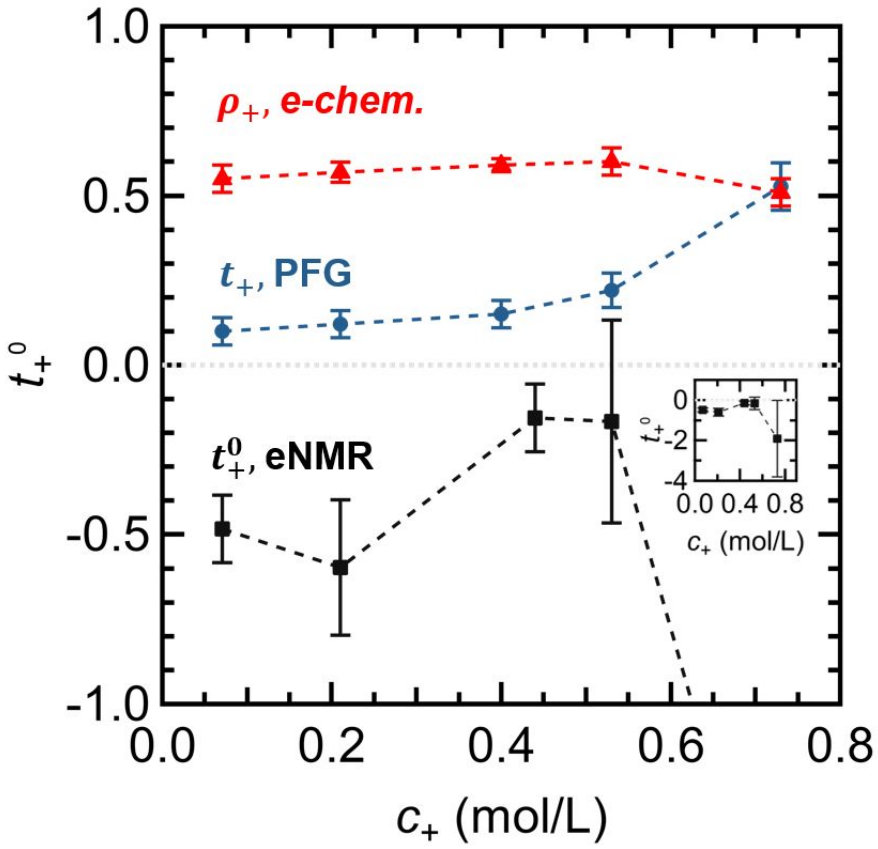

Figure 7. Comparison of transference number measured as a function of salt concentration at 30 °C using three independent methods. Current fraction (ρ_+) measured electrochemically (up triangle, red), transference number measured by PFG-NMR method ($t_{+,PFG}$) (circle, blue) and transference number measured by eNMR technique (t_+^0) (square, black). The inset represents t_+^0 at the highest salt concentration.

Conclusions

We studied lithium transference in a multivalent electrolyte containing a bulky star-shaped anion with $z_- =$ -20 using three experimental techniques: electrochemical polarization (ρ_+), PFG-NMR ($t_{+,PFG}$) and electrophoretic NMR (t_+^0). Interest in such electrolytes arises due to the possibility of improving lithium transference by slowing down the mobility of the anion. In univalent electrolytes, the self-diffusion coefficient of lithium ions is much smaller than that of the anions. In our multivalent electrolyte, PFG-NMR shows that the reverse is true – the self-diffusion

coefficient of the cation is higher than that of the anions at all salt concentrations. Electrochemical polarization experiments show that the multivalent electrolytes are able to sustain a higher current than that expected from PFG-NMR. The cation transference number with respect to the solvent velocity, t_+^0, is negative at all salt concentrations indicating that cation transference does not necessarily reflect the slowing down of the self-diffusion coefficient of the anion. Similar effects were reported by Fong et al. in solutions of linear multivalent anions with lithium counterions.[19,60] Recently, using eNMR, Bergstrom et al. showed that t_+^0 was negative for these systems.[23] It is evident that ion transport in our multivalent electrolytes depends on additional parameters such as the activity of the multivalent salt, and the diffusion coefficient measured by approaches such as restricted diffusion. In addition, computer simulations that account for anion–solvent, cation–solvent and cation–anion correlations are necessary to understand the molecular underpinnings of ion transport in electrolytes with multivalent star-shaped ions.

Author contributions

The manuscript was written through contributions of all authors. All the authors gave approval to the final version of the manuscript. S.C. and D.M.H. contributed equally.

Conflict of interest

There are no conflicts of interest to declare.

Acknowledgements

This work was fully supported by the Joint Center for Energy Storage Research (JCESR), an Energy Innovation Hub funded by the U.S. Department of Energy, Office of Science, Basic Energy Sciences. We thank Dr. Hasan Celik and UC Berkeley's NMR facility in the College of Chemistry (CoC-NMR) for spectroscopic assistance. The NMR instrument used in this work was supported by the National Science Foundation under Grant No. 2018784. We thank Helen Bergstrom for the helpful scientific input.

References

(1) Nguyen, T. K. L.; Phan, T. N. T.; Cousin, F.; Devaux, D.; Mehan, S.; Ziarelli, F.; Viel, S.; Gigmes, D.; Soudant, P.; Bouchet, R. Polyhedral Oligomeric Silsesquioxane-Based Macroanions to Level Up the Li+Transport Number of Electrolytes for Lithium Batteries.

Chemistry of Materials **2022**, *34*, 6944–6957.

(2) Darling, R. M.; Gallagher, K. G.; Kowalski, J. A.; Ha, S.; Brushett, F. R. Pathways to Low-Cost Electrochemical Energy Storage: A Comparison of Aqueous and Nonaqueous Flow Batteries. *Energy and Environmental Science* **2014**, *7*, 3459–3477.

(3) Rodby, K. E.; Carney, T. J.; Ashraf Gandomi, Y.; Barton, J. L.; Darling, R. M.; Brushett, F. R. Assessing the Levelized Cost of Vanadium Redox Flow Batteries with Capacity Fade and Rebalancing. *Journal of Power Sources* **2020**, *460*, 227958.

(4) Lau, K.-C.; Seguin, T. J.; Carino, E. V.; Hahn, N. T.; Connell, J. G.; Ingram, B. J.; Persson, K. A.; Zavadil, K. R.; Liao, C. Widening Electrochemical Window of Mg Salt by Weakly Coordinating Perfluoroalkoxyaluminate Anion for Mg Battery Electrolyte. *Journal of The Electrochemical Society* **2019**, *166*, A1510–A1519.

(5) Hahn, N. T.; McClary, S. A.; Landers, A. T.; Zavadil, K. R. Efficacy of Stabilizing Calcium Battery Electrolytes through Salt-Directed Coordination Change. *Journal of Physical Chemistry C* **2022**, *126*, 10335–10345.

(6) Self, J.; Hahn, N. T.; Fong, K. D.; McClary, S. A.; Zavadil, K. R.; Persson, K. A. Ion Pairing and Redissociaton in Low-Permittivity Electrolytes for Multivalent Battery Applications. *Journal of Physical Chemistry Letters* **2020**, *11*, 2046–2052.

(7) Nyman, A.; Behm, M.; Lindbergh, G. Electrochemical Characterisation and Modelling of the Mass Transport Phenomena in LiPF6-EC-EMC Electrolyte. *Electrochimica Acta* **2008**, *53*, 6356–6365.

(8) Landesfeind, J.; Gasteiger, H. A. Temperature and Concentration Dependence of the Ionic Transport Properties of Lithium-Ion Battery Electrolytes. *Journal of The Electrochemical Society* **2019**, *166*, A3079–A3097.

(9) Geiculescu, O. E.; Rajagopal, R.; Creager, S. E.; DesMarteau, D. D.; Zhang, X.; Fedkiw, P. Transport Properties of Solid Polymer Electrolytes Prepared from Oligomeric Fluorosulfonimide Lithium Salts Dissolved in High Molecular Weight Poly(Ethylene Oxide). *Journal of Physical Chemistry B* **2006**, *110*, 23130–23135.

(10) Kreuer, Klaus. D.; Wohlfarth, A.; Araujo, C. C.; Fuchs, A.; Maier, J. Single Ion Li+ Na+

Conductors by Ion Exchange of Proton-Conducting Ionomers and Polyelectrolytes_SI_Maier_2011. *Chem. Phys. Chem.* **2011**, *12*, 2558.

(11) Qiao, B.; Leverick, G. M.; Zhao, W.; Flood, A. H.; Johnson, J. A.; Shao-Horn, Y. Supramolecular Regulation of Anions Enhances Conductivity and Transference Number of Lithium in Liquid Electrolytes. *Journal of the American Chemical Society* **2018**, *140*, 10932–10936.

(12) Newman, J.; Balsara, N. P. *Electrochemical Systems*, Fourth Edi.; Wiley: Hoboken, 2021.

(13) Onsager, L. Reciprocal Relations in Irreversible Processes. I. *Phys. Rev.* **1931**, *37*, 405.

(14) Onsager, L. Reciprocal Relations in Irreversible Processes. II. *Phys. Rev.* **1931**, *38*, 2265.

(15) Bruce, P. G.; Vincent, C. A. Steady State Current Flow in Solid Binary Electrolyte Cells. *Journal of Electroanalytical Chemistry* **1987**, *225*, 1–17.

(16) Evans, J.; Vincent, C. A.; Bruce, P. G. Electrochemical Measurement of Transference Numbers in Polymer Electrolytes. *Polymer* **1987**, *28*, 2324–2328.

(17) Watanabe, M.; Nagano, S.; Sanui, K.; Ogata, N. Estimation of Li+ Transport Number in Polymer Electrolytes by the Combination of Complex Impedance and Potentiostatic Polarization Measurements. *Solid State Ionics* **1988**, *30*, 911–917.

(18) Hayamizu, K.; Akiba, E.; Bando, T.; Aihara, Y. 1H, 7Li, and 19F Nuclear Magnetic Resonance and Ionic Conductivity Studies for Liquid Electrolytes Composed of Glymes and Polyetheneglycol Dimethyl Ethers of CH3O(CH2CH2O)NCH3 (n = 3 - 50) Doped with LiN(SO2CF3)2. *Journal of Chemical Physics* **2002**, *117*, 5929–5939.

(19) Fong, K. D.; Self, J.; Diederichsen, K. M.; Wood, B. M.; McCloskey, B. D.; Persson, K. A. Ion Transport and the True Transference Number in Nonaqueous Polyelectrolyte Solutions for Lithium Ion Batteries. *ACS Central Science* **2019**, *5*, 1250–1260.

(20) Grundy, L. S.; Shah, D. B.; Nguyen, H. Q.; Diederichsen, K. M.; Celik, H.; DeSimone, J. M.; McCloskey, B. D.; Balsara, N. P. Impact of Frictional Interactions on Conductivity, Diffusion, and Transference Number in Ether- and Perfluoroether-Based Electrolytes. *Journal of The Electrochemical Society* **2020**, *167*, 120540.

(21) Gao, K. W.; Fang, C.; Halat, D. M.; Mistry, A.; Newman, J.; Balsara, N. P. The Transference Number. *Energy and Environmental Materials* **2022**, *5*, 366–369.

(22) Balsara, N. P.; Newman, J. Divergence of Velocity Fields in Electrochemical Systems Divergence of Velocity Fields in Electrochemical Systems. *J. Electrochem. Soc.* **2022**, *169*, 070535.

(23) Bergstrom, H. K.; Fong, K. D.; Halat, D. M.; Karouta, C. A.; Celik, H. C.; Reimer, J. A.; McCloskey, B. D. Ion Correlation and Negative Lithium Transference in Polyelectrolyte Solutions. *Chem. Sci.* **2023**, 10.1039.D3SC01224G.

(24) Timachova, K.; Newman, J.; Balsara, N. P. Theoretical Interpretation of Ion Velocities in Concentrated Electrolytes Measured by Electrophoretic NMR. *Journal of The Electrochemical Society* **2019**, *166*, A264–A267.

(25) Halat, D. M.; Fang, C.; Hickson, D.; Mistry, A.; Reimer, J. A.; Balsara, N. P.; Wang, R. Electric-Field-Induced Spatially Dynamic Heterogeneity of Solvent Motion and Cation Transference in Electrolytes. *Physical Review Letters* **2022**, *128*.

(26) Giesecke, M.; Mériguet, G.; Hallberg, F.; Fang, Y.; Stilbs, P.; Furó, I. Ion Association in Aqueous and Non-Aqueous Solutions Probed by Diffusion and Electrophoretic NMR. *Physical Chemistry Chemical Physics* **2015**, *17*, 3402–3408.

(27) Dai, H.; Zawodzinski, T. A. The Dependence of Lithium Transference Numbers on Temperature, Salt Concentration and Anion Type in Poly (Vinylidene Fluoride)-Hexafluoropropylene Copolymer-Based Gel Electrolytes. *Journal of Electroanalytical Chemistry* **1998**, *459*, 111–119.

(28) Walls, H. J.; Zawodzinski, T. A. Anion and Cation Transference Numbers Determined by Electrophoretic NMR of Polymer Electrolytes Sum to Unity. *Electrochemical and Solid-State Letters* **2000**, *3*, 321–324.

(29) Schmidt, F.; Schönhoff, M. Solvate Cation Migration and Ion Correlations in Solvate Ionic Liquids. *Journal of Physical Chemistry B* **2020**, *124*, 1245–1252.

(30) Wang, A. A.; Gunnarsdóttir, A. B.; Fawdon, J.; Pasta, M.; Grey, C. P.; Monroe, C. W. Potentiometric MRI of a Superconcentrated Lithium Electrolyte: Testing the Irreversible

Thermodynamics Approach. *ACS Energy Letters* **2021**, *6*, 3086–3095.

(31) Brinkkötter, M.; Giffin, G. A.; Moretti, A.; Jeong, S.; Passerini, S.; Schönhoff, M. Relevance of Ion Clusters for Li Transport at Elevated Salt Concentrations in [Pyr12O1][FTFSI] Ionic Liquid-Based Electrolytes. *Chemical Communications* **2018**, *54*, 4278–4281.

(32) Nürnberg, P.; Atik, J.; Borodin, O.; Winter, M.; Paillard, E.; Schönhoff, M. Superionicity in Ionic-Liquid-Based Electrolytes Induced by Positive Ion-Ion Correlations. *Journal of the American Chemical Society* **2022**, *144*, 4657–4666.

(33) Huang, Q. R.; Dubin, P. L.; Moorefield, C. N.; Newkome, G. R. Counterion Binding on Charged Spheres: Effect of PH and Ionic Strength on the Mobility of Carboxyl-Terminated Dendrimers. *J. Phys. Chem. B* **2000**, *104*, 898–904.

(34) Seyrek, E.; Dubin, P. L.; Newkome, G. R. Effect of Electric Field on the Mobility of Carboxyl-Terminated Dendrimers. *J. Phys. Chem. B* **2004**, *108*, 10168–10171.

(35) Hsu, J.-P.; Lin, C.-Y.; Yeh, L.-H.; Lin, S.-H. Influence of the Shape of a Polyelectrolyte on Its Electrophoretic Behavior. *Soft Matter* **2012**, *8*, 9469–9479.

(36) Gopmandal, P. P.; Bhattacharyya, S. Nonlinear Effects on Electrokinetics of a Highly Charged Porous Sphere. *Colloid Polym Sci* **2014**, *292*, 905–914.

(37) Welch, C. F.; Hoagland, D. A. The Electrophoretic Mobility of PPI Dendrimers: Do Charged Dendrimers Behave as Linear Polyelectrolytes or Charged Spheres? *Langmuir* **2003**, *19*, 1082–1088.

(38) Moussa, M.; Caillet, C.; Town, R. M.; Duval, J. F. L. Remarkable Electrokinetic Features of Charge-Stratified Soft Nanoparticles: Mobility Reversal in Monovalent Aqueous Electrolyte. *Langmuir* **2015**, *31*, 5656–5666.

(39) Villaluenga, I.; Chen, X. C.; Devaux, D.; Hallinan, D. T.; Balsara, N. P. Nanoparticle-Driven Assembly of Highly Conducting Hybrid Block Copolymer Electrolytes. *Macromolecules* **2015**, *48*, 358–364.

(40) Spees, W. M.; Song, S.-K.; Garbow, J. R.; Neil, J. J.; Ackerman, J. J. H. Use of Ethylene

Glycol to Evaluate Gradient Performance in Gradient-Intensive Diffusion MR Sequences. *Magn. Reson. Med.* **2012**, *68*, 319–324.

(41) Fang, Y.; Yushmanov, P. V.; Furó, I. Improved Accuracy and Precision in Electrophoretic NMR Experiments. Current Control and Sample Cell Design. *Journal of Magnetic Resonance* **2020**, *318*, 106796.

(42) Jerschow, A.; Müller, N. Convection Compensation in Gradient Enhanced Nuclear Magnetic Resonance Spectroscopy. *Journal of Magnetic Resonance* **1998**, *132*, 13–18.

(43) He, Q.; Wei, Z. Convection Compensated Electrophoretic NMR. *Journal of Magnetic Resonance* **2001**, *150*, 126–131.

(44) Pettersson, E.; Furó, I.; Stilbs, P. On Experimental Aspects of Electrophoretic NMR. *Concepts in Magnetic Resonance Part A: Bridging Education and Research* **2004**, *22*, 61–68.

(45) Zhang, Z.; Madsen, L. A. Observation of Separate Cation and Anion Electrophoretic Mobilities in Pure Ionic Liquids. *Journal of Chemical Physics* **2014**, *140*.

(46) Wheeler, D. R.; Newman, J. Molecular Dynamics Simulations of Multicomponent Diffusion. 1. Equilibrium Method. *J. Phys. Chem. B* **2004**, *108*, 18353–18361.

(47) France-Lanord, A.; Grossman, J. C. Correlations from Ion Pairing and the Nernst-Einstein Equation. *Phys. Rev. Lett.* **2019**, *122*, 136001.

(48) Fong, K. D.; Bergstrom, H. K.; McCloskey, B. D.; Mandadapu, K. K. Transport Phenomena in Electrolyte Solutions: Nonequilibrium Thermodynamics and Statistical Mechanics. *AIChE J.* **2020**, *66*, e17091.

(49) Fang, C.; Mistry, A.; Srinivasan, V.; Balsara, N. P.; Wang, R. Elucidating the Molecular Origins of the Transference Number in Battery Electrolytes Using Computer Simulations. *JACS Au* **2023**, jacsau.2c00590.

(50) Mongcopa, K. I. S.; Gribble, D. A.; Loo, W. S.; Tyagi, M.; Mullin, S. A.; Balsara, N. P. Segmental Dynamics Measured by Quasi-Elastic Neutron Scattering and Ion Transport in Chemically Distinct Polymer Electrolytes. *Macromolecules* **2020**, *53*, 2406–2411.

(51) Hickson, D. T.; Halat, D. M.; Ho, A. S.; Reimer, J. A.; Balsara, N. P. Complete Characterization of a Lithium Battery Electrolyte Using a Combination of Electrophoretic NMR and Electrochemical Methods. *Physical Chemistry Chemical Physics* **2022**, *24*, 26591–26599.

(52) Yoshida, K.; Tsuchiya, M.; Tachikawa, N.; Dokko, K.; Watanabe, M. Change from Glyme Solutions to Quasi-Ionic Liquids for Binary Mixtures Consisting of Lithium Bis(Trifluoromethanesulfonyl)Amide and Glymes. *Journal of Physical Chemistry C* **2011**, *115*, 18384–18394.

(53) Hou, T.; Monroe, C. W. Composition-Dependent Thermodynamic and Mass-Transport Characterization of Lithium Hexafluorophosphate in Propylene Carbonate. *Electrochimica Acta* **2020**, *332*, 135085.

(54) Craig, N.; Mullin, S. A.; Pratt, R.; Crane, G. B. Determination of Transference Number and Thermodynamic Factor by Use of Anion-Exchange Concentration Cells and Concentration Cells. *Journal of The Electrochemical Society* **2019**, *166*, A2769–A2775.

(55) Manning, G. S. Nonconvective Ionic Flow in Fixed-Charge Systems. *The Journal of Chemical Physics* **1967**, *46*, 2324–2333.

(56) Manning, G. S. Limiting Laws and Counterion Condensation in Polyelectrolyte Solutions II. Self-Diffusion of the Small Ions. *The Journal of Chemical Physics* **1969**, *51*, 934–938.

(57) Manning, G. S. Molecular Theory of Counterion Conductivity and Self-Diffusion in Polyelectrolyte Solutions. *The Journal of Chemical Physics* **1967**, *47*, 2010–2013.

(58) Böhme, U.; Scheler, U. Effective Charge of Poly(Styrenesulfonate) and Ionic Strength - An Electrophoresis NMR Investigation. *Colloids and Surfaces A: Physicochemical and Engineering Aspects* **2003**, *222*, 35–40.

(59) Böhme, U.; Klenge, A.; Hänel, B.; Scheler, U. Counterion Condensation and Effective Charge of PAMAM Dendrimers. *Polymers* **2011**, *3*, 812–819.

(60) Fong, K. D.; Self, J.; McCloskey, B. D.; Persson, K. A. Ion Correlations and Their Impact on Transport in Polymer-Based Electrolytes. *Macromolecules* **2021**, *54*, 2575–2591.